Field Line Resonances in Jupiter's Magnetosphere

R. L. Lysak[1] and Y. Song[1]

[1]Minnesota Institute for Astrophysics, School of Physics and Astronomy, University of Minnesota, Minneapolis, MN, USA.

Key Points:

- Alfvén wave field line resonances are described in a model of Jupiter's magnetosphere
- These resonances occur with periods of 10-40 minutes
- These waves are consistent with measurements of magnetic fluctuations in Jupiter's magnetosphere, as well as with oscillations in auroral luminosity

Abstract

The arrival of the Juno satellite at Jupiter has led to an increased interest in the dynamics of the Jovian magnetosphere. Jupiter's auroral emissions often exhibit quasi-periodic oscillations with periods of tens of minutes. Magnetic observations indicate that ultra-low-frequency (ULF) waves with similar periods are often seen in data from Galileo and other satellites traversing the Jovian magnetosphere. Such waves can be associated with field line resonances, which are standing shear Alfvén waves on the field lines. Using model magnetic fields and plasma distributions, the frequencies of field line resonances and their harmonics on field lines connecting to the main auroral oval have been determined. Time domain simulations of Alfvén wave propagation have illustrated the evolution of such resonances. These studies indicate that harmonics of the field line resonances are common in the 10-40 minute band.

Plain Language Summary:

The magnetic field lines of planets like Earth and Jupiter can act like the strings of a musical instrument, and can support waves at specific frequencies in the same way that a guitar or violin string has a particular frequency. The rapid rotation of Jupiter causes its field line to be stretched out, and the volcanos on Jupiter's moon Io produces a dense plume of ionized gas (plasma) that populates these stretched field lines. By making a numerical model of Jupiter's magnetic field and plasma, we have calculated the frequencies of these field lines, which have much lower frequencies than a musical instrument so that the periods are tens of minutes. This period corresponds to oscillations in the visible aurora (northern and southern lights) at Jupiter.

Index terms: 2752 MHD Waves and Instabilities, 2756 Planetary Magnetospheres, 5734 Magnetic Fields and Magnetism, 2753 Numerical Modeling

Key Words: Field line resonances, Magnetic Modeling, Quasi-periodic oscillations, Jupiter

1. Introduction

One goal of the NASA Juno mission, in polar orbit around Jupiter, is the investigation of auroral processes in the magnetosphere of this giant planet (e.g., Bagenal et al., 2014). One of the features of the Jovian aurora is the appearance of quasi-periodic variations in auroral intensity with periods of tens of minutes. Variations with a period of about 10 minutes have been observed by the Hubble Space Telescope (Nichols, 2017) in the ultra-violet, by the Japanese Subaru satellite (Watanabe et al., 2018) in the infrared, and in X-rays from Chandra and XMM-Newton (Dunn et al., 2017). In situ observations at Jupiter have indicated that magnetic fluctuations in the 10-20 minute range were present in Voyager 2 data (Khurana & Kivelson, 1989). Similar observations were made by Galileo (Manners et al., 2018; Manners & Masters, 2019; Wilson & Dougherty, 2000). In addition, Alfvén waves have long been associated with the coupling of the moon Io with the ionosphere of Jupiter (e.g., Bagenal, 1983; Belcher et al., 1981; Chust et al., 2005; Crary, 1997; Gurnett & Goertz, 1981; Hinton et al., 2019); however, the focus of this letter will be on the main auroral oval.

Modeling of the Jovian Alfvén waves was first considered using a simplified box model (Khurana & Kivelson, 1989) in which the magnetic field lines are "straightened out" and the two conjugate ionospheres are planes perpendicular to the field lines. In their model, the plasma sheet of Jupiter was modeled by a slab of enhanced density in the equatorial plane. Otherwise the magnetic field was constant and the density is constant outside of the slab. This type of model has recently been taken up by Manners et al. (2018) and Manners and Masters (2019) who compared the results of the box model calculations to data from Galileo by adjusting the Alfvén speed and the plasma sheet thickness to fit the data.

However, the box model is oversimplified in that it does not include the realistic geometry and distribution of plasma along the field line. In the terrestrial magnetosphere, models using a dipole geometry have been used to calculate the resonant periods of magnetospheric field lines (e.g., Cummings et al., 1969). Furthermore, finite difference time domain models using dipole geometry have also been used (e.g., Lee & Lysak, 1989, 1990, 1991; Streltsov and Lotko, 1997; Rankin et al., 1999; Tikhonchuk & Rankin, 2000) to model ULF waves in the magnetosphere. However, the field lines connecting to the main auroral oval at Jupiter are clearly on field lines that are far from dipolar, due to the magnetodisk of plasma that is emitted from the moon Io (e.g., Bagenal, 1994).

The purpose of this letter is to study ultra-low-frequency (ULF) waves in the Jovian magnetosphere in a more realistic model of the magnetic field. The magnetic field in this model is based on Connerney et al. (1981) who considered the field due to a current sheet of finite thickness and radial extent in addition to the internal, dipolar magnetic field of the planet. It should be noted that close approach of Juno to Jupiter have allowed for the modeling of the higher order multipoles of the magnetic field (Connerney et al., 2018); however, these higher multipoles fall off faster than the dipolar contribution at large distances from Jupiter. Since the frequency of the field line resonance is largely controlled by the outer parts of the field line, a dipole model for the internal contribution to the magnetic field will suffice for our study.

In addition to a magnetic field model, we require a model of the plasma mass density to calculate the Alfvén speed. We have adopted the model of Bagenal and Delamere (2011) based on Voyager and Galileo data. This model describes the plasma density and temperature profile beyond Io's orbit, assuming a constant average ion mass. The plasma sheet in this work is assumed to decay as a Gaussian with a scale height dependent on the temperature, which increases with radial distance from Jupiter. Further analysis of the Voyager data by Dougherty et al. (2017) has provided a detailed breakdown of the heavy ions in the system, and has shown an electron density about a factor of 4 higher than the Bagenal and Delamere (2011) results.

The remainder of this letter is organized as follows: First, we will discuss details of the background magnetic field and density models used in this work. Then, we will describe the coordinate system used and the equations used to calculate the field line resonant frequencies. After showing the results, we will show initial results from time-domain simulations of the propagation of the Alfvén waves along the Jovian magnetic field lines. We will conclude with a discussion of the results and plans for future work.

2. Magnetic Field and Plasma Models

The CAN81 model (Connerney et al., 1981) starts by assuming a current sheet extending outward for radial distances $\rho > a$ from the dipole axis (in cylindrical coordinates), and extending from $z = -D$ to $z = D$. The current in this sheet is assumed to vary as $1/\rho$. Then the Green's function for the current sheet being at z' is given by

$$G(\rho, z, z') = \frac{\mu_0}{2} \int_0^\infty \frac{d\lambda}{\lambda} J_1(\lambda\rho) J_0(\lambda a) e^{-\lambda|z-z'|} \tag{1}$$

Then the vector potential can be written as

$$A_\varphi(\rho, z) = \int_{-D}^{D} dz' G(\rho, z, z') j_\varphi(z') \tag{2}$$

The current density is given by $j_\varphi(\rho, z') = I_\varphi(z')/\rho$. Assuming that $I_\varphi(z') = I_0$ for $|z'| < D$ and 0 elsewhere, the vector potential becomes

$$A_\varphi = \mu_0 I_0 \int_0^\infty \frac{d\lambda}{\lambda^2} J_1(\lambda\rho) J_0(\lambda a) \sinh(\lambda D) e^{-\lambda|z|} \tag{3}$$

for $|z| > D$, and for $|z| < D$:

$$A_\varphi = \mu_0 I_0 \int_0^\infty \frac{d\lambda}{\lambda^2} J_1(\lambda\rho) J_0(\lambda a) \left[1 - e^{-\lambda D} \cosh \lambda z\right] \tag{4}$$

As a further refinement, the current sheet can be assumed to extend from $\rho = a_1$ to $\rho = a_2$, which modifies equations (3) and (4) to read:

$$A_\varphi = \mu_0 I_0 \int_0^\infty \frac{d\lambda}{\lambda^2} J_1(\lambda\rho) \left[J_0(\lambda a_1) - J_0(\lambda a_2)\right] \sinh(\lambda D) e^{-\lambda|z|} \tag{5}$$

$$A_\varphi = \mu_0 I_0 \int_0^\infty \frac{d\lambda}{\lambda^2} J_1(\lambda\rho) \left[J_0(\lambda a_1) - J_0(\lambda a_2)\right] \left[1 - e^{-\lambda D} \cosh \lambda z\right] \tag{6}$$

This field is added to the vector potential for a dipole, which is given in cylindrical coordinates as

$$A_{\varphi,dip} = B_0 R_J^3 \frac{\sin\theta}{r^2} = B_0 R_J^3 \frac{\rho}{\left(\rho^2 + z^2\right)^{3/2}} \tag{7}$$

In this expression, $B_0 = 430$ μT is the equatorial surface field at Jupiter and $R_J = 71{,}492$ km is the 1 bar radius of the planet (e.g., Bagenal et al., 2014). Then the magnetic field components can be computed by taking the curl of the vector potential as usual. Explicit forms for the magnetic field are given by Connerney et al. (1981).

This vector potential can be used to create a coordinate system using the so-called Euler potentials, $\mathbf{B} = \nabla\alpha \times \nabla\beta$, where β is the azimuthal coordinate and $\alpha = \rho A_\varphi$ is sometimes called the flux function, since it is proportional to the amount of magnetic flux enclosed by the field line. Following Connerney et al. (1981), we will adopt this model with $a_1 = 5\ R_J$, $a_2 = 50\ R_J$ and $D = 2.5\ R_J$, with a current of $I_0 = 25.6\times10^6$ A/R_J, corresponding to $\mu_0 I_0 = 450$ nT. This model was fit to measurements from Voyager 1 and Pioneer 10.

With the magnetic geometry being defined, we next need to adopt a model for the plasma mass density, which is necessary to compute the Alfvén speed. As a first model, we will adopt the plasma sheet model described by Bagenal and Delamere (2011) based on Galileo data. In their model, the equatorial density outside of Io's orbit (at about 6 R_J) is given by

$$n_0(\mathrm{cm}^{-3}) = 1987(r/6)^{-8.2} + 14\left(r/6\right)^{-3.2} + 0.05\left(r/6\right)^{-0.65} \qquad r > 6 \tag{8}$$

Here r is measured in Jovian radii. Since the plasma density is expected to fall off rapidly inside Io's orbit, we have taken the density in this region to vary as

$$n_0\left(\mathrm{cm}^{-3}\right) = 2001.05\exp\left(-\left(\frac{r/6-1}{0.1}\right)^2\right) \tag{9}$$

Away from the equator, Bagenal and Delamere (2011) assume a Gaussian fall-off to the density:

$$n\left(\rho, z\right) = n_0\left(\rho\right)e^{-(z/H)^2} \tag{10}$$

Where $H = H_0\sqrt{T_i(\mathrm{eV})/M}$ with $H_0 = 0.64\ R_J$ and M is the average ion mass in units of the proton mass. The average ion temperature is assumed to follow

$$h = -0.116 + 2.14r - 2.05r^2 + 0.491r^3 + 0.126r^4 \tag{11}$$

Heree $h = \log_{10} H$ and $r = \log_{10}\rho$ and again, H and ρ are measured in Jovian radii. The average mass of the plasma sheet ions is taken to be 20 amu, in agreement with Bagenal and Delamere (2011). Finally, the ionosphere is taken protons, with an exponential profile:

$$n_I = n_{I0}e^{-r/H_I} \tag{12}$$

With $n_{I0} = 2\times10^5$ cm^{-3} and $H_I = 4200$ km, as in the work of Su et al. (2006). In addition to these populations, the background density in the tail is restricted to a minimum value of 0.01 cm^{-3}. Figure 1a shows the magnetic field profile in the model runs, with Figure 1b being the mass density profile and Figure 1c showing the Alfvén speed determined from the magnetic field and density. Each of these plots also includes representative field lines at M = 10, 15, 20, 25, 30 and 35, where M gives the equatorial crossing of the field line in units of Jovian radii (Allegrini et al., 2017).

3. Calculation of the field line resonance frequencies

Using the background parameters given in the previous section, we can then calculate the resonant frequencies on each field line. This is a well-established procedure in terrestrial magnetospheric

physics, going back to the seminal work of Cummings et al. (1969). Here we assume that the waves are governed by the ideal MHD equations for shear Alfvén waves. The Euler potentials α and β serve as coordinates that define a field line, and we take the length *s* along the field line to be the third coordinate. We will focus on toroidal modes (in which the velocity and magnetic perturbations are in the azimuthal direction), since the observations of Manners and Masters (2019) indicate that this mode is dominant. The toroidal mode has only two non-zero fields, E_α and B_β, which correspond to the radial and azimuthal components, respectively, at the equatorial plane. Then the equations for the shear Alfvén mode can be written as

$$\frac{\partial E_\alpha}{\partial t} = -\frac{c_A^2}{h_\beta}\frac{\partial\left(h_\beta B_\beta\right)}{\partial s} \qquad (13)$$

$$\frac{\partial B_\beta}{\partial t} = -\frac{1}{h_\alpha}\frac{\partial\left(h_\alpha E_\alpha\right)}{\partial s} \qquad (14)$$

In these equations, $c_A^2 = V_A^2/\left(1+V_A^2/c^2\right)$, where $V_A^2 = B^2/\mu_0 nM$ is the non-relativistic MHD Alfvén speed and h_α and h_β are scale factors. Since α and β define field lines, the area of a flux tube is proportional to $h_\alpha h_\beta$, and so $h_\alpha h_\beta \sim 1/B$. The azimuthal coordinate β has a scale factor $h_\beta = r\sin\theta$ in spherical coordinates or $h_\beta = \rho$ in cylindrical coordinates, so the other scale factor $h_\alpha = R_J^2 B_0 / h_\beta B$.

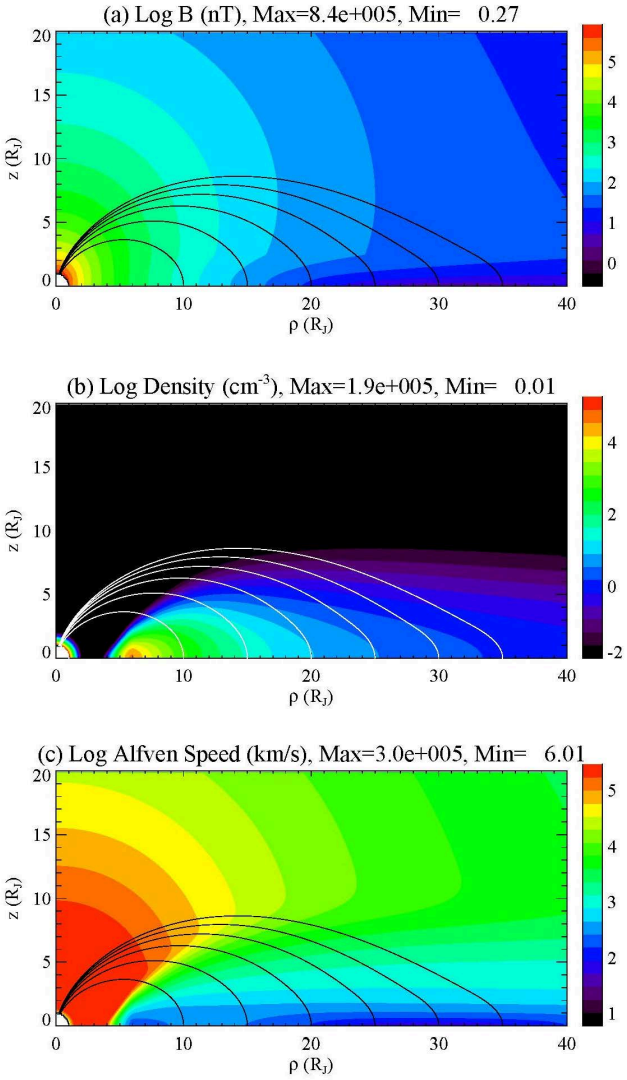

Figure 1. Background parameters for the eigenfrequency calculation. (a) Magnetic Field; (b) Mass density; (c) Alfvén speed. Contours in each plot are magnetic field lines.

To determine the field line resonances, equations (13) and (14) are Fourier transformed in time and integrated from one ionosphere to the other. It is convenient to incorporate the scale factors into the fields and to recognize that in a standing wave the electric and magnetic fields are in quadrature, so we define the variables as $\tilde{E} = h_\alpha E_\alpha$ and $\tilde{B} = ih_\beta B_\beta$. In terms of these variables, these equations become

$$\frac{\partial \tilde{E}}{\partial s} = \omega\frac{h_\alpha}{h_\beta}\tilde{B} \qquad \frac{\partial \tilde{B}}{\partial s} = \frac{\omega}{c_A^2}\frac{h_\beta}{h_\alpha}\tilde{E} \qquad (15)$$

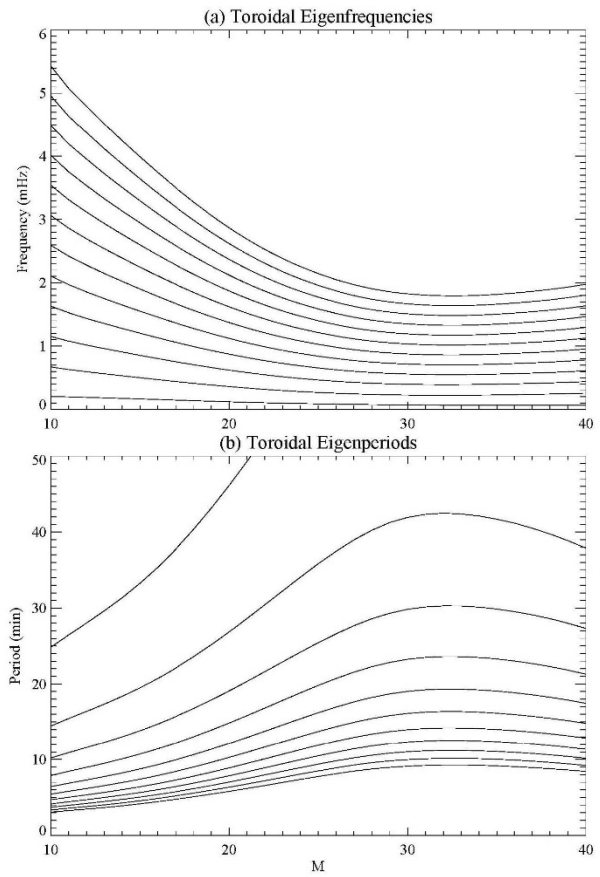

Figure 2. Eigenfrequencies as a function of M-shell for first 12 eigenmodes. (a) Frequencies in mHz; (b) Periods in minutes. Note that the fundamental mode, which has periods greater than 80 minutes for all values of M, is not shown in this panel.

Next we must introduce boundary conditions. The ionosphere is estimated to have a Pedersen conductance in the auroral zone of 0.5 S (e.g., Yates et al., 2014), while the characteristic Alfvén impedance, $Z_A = \mu_0 c_A$, is 377 Ω since c_A approaches the speed of light. In the terrestrial magnetosphere, it is well known that the ionospheric electric field becomes very small when $Z_A \Sigma_P >> 1$ (e.g., Mallinckrodt & Carlson, 1978), and so we can assume the electric field goes to zero at the boundary. So equations (15) are integrated starting at one ionosphere with $\tilde{E} = 0$ and $\tilde{B}$ arbitrarily set to 1. Then the equations are integrated for varying values of ω until a solution with $\tilde{E} = 0$ at the other ionosphere is satisfied using a shooting method (e.g., Press et al., 1992).

Results for the first 12 modes are shown in Figure 2. Figure 2a shows the eigenfrequencies, in milliHertz, for these modes as a function of the M-value. Figure 2b shows the same information, but in terms of the periods of the waves in minutes. Note that the fundamental mode, which has a period greater than 80 minutes for all values of M, is not shown in Figure 2b, so that the longest period shown, with a period of 25 minutes at M = 10, is the second mode (or the first harmonic). It can be seen from this figure that there are multiple modes in the 10-40 minute range typical of the quasi-periodic oscillations in the aurora. It is interesting to note that while the periods tend to increase with increasing M, which is not surprising since these field lines are longer, at the largest values of M, the period decreases somewhat. This is due to the fact that these field lines sample the region where the Alfvén speed approaches the speed of light, which can be seen in Figure 1c.

Next, we should consider the wave forms associated with these eigenmodes. Since there are multiple harmonics in the region of interest and a wide variety of field lines to consider, we will be guided by the observations of Manners and Masters (2019), who observed a number of resonant modes by the Galileo satellite. Their observations occurred near the equatorial plane at a radial distance of 23 R_J, so the M = 23 field line is appropriate. They observed resonant toroidal modes with periods of about 22, 14, 7 and 4 minutes. In the model magnetosphere considered here, these

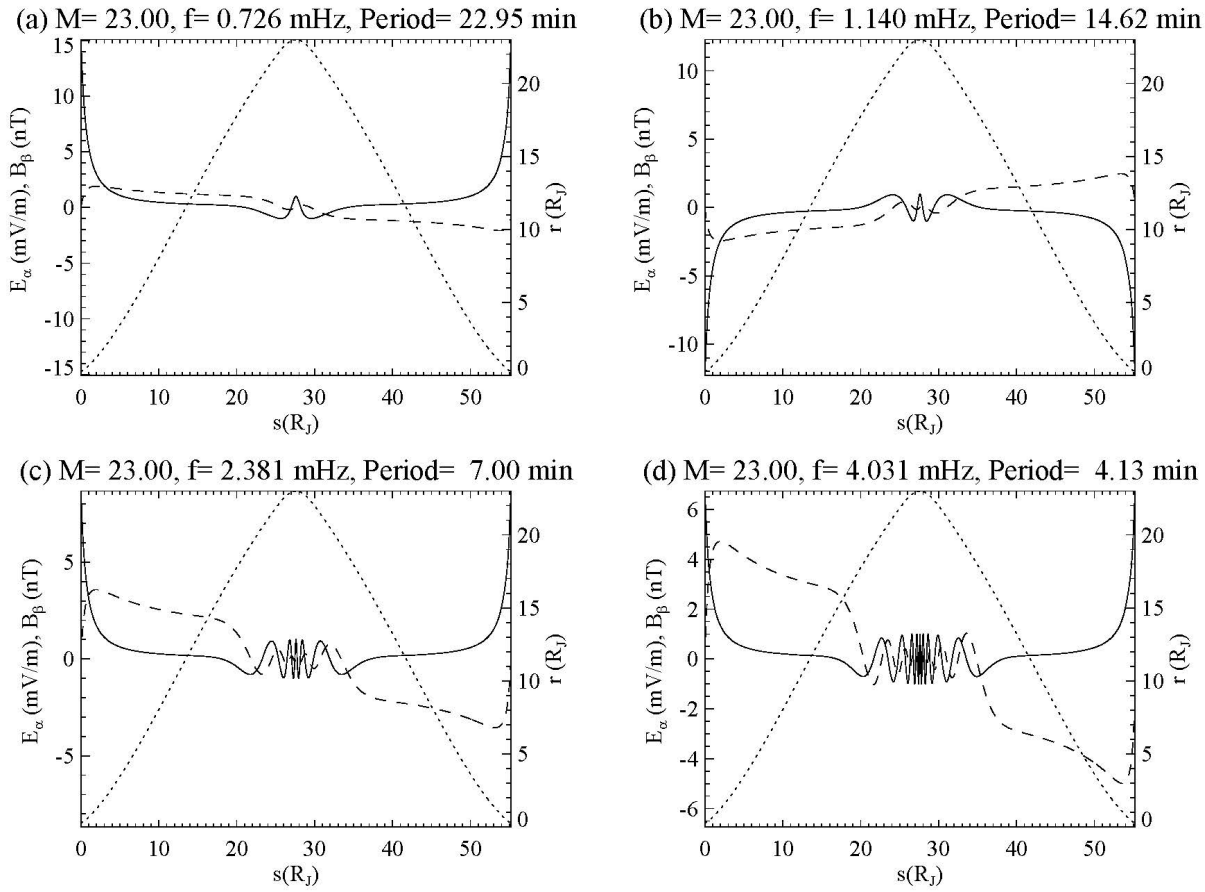

Figure 3. Eigenfunctions for selected modes at M = 23 as a function of length along the field line. Solid curves give magnetic perturbations and dashed curves are electric field perturbation. The fields are normalized so that the wave magnetic field at the equator is 1 nT. The dotted curve gives the radial distance of each point, referenced to the right-hand scale. (a) Mode 4, period of 22.9 minutes; (b) Mode 6, period of 14.6 minutes; (c) Mode 12, period of 7.0 minutes; (d) Mode 22, period of 4.1 minutes.

correspond roughly to the mode numbers 4 (22.9 minutes), 6 (14.6 minutes), 12 (7.0 minutes) and 20 (4.1 minutes). The wave forms for these modes are shown in Figure 3. In this figure, the magnetic perturbation is given by the solid curve and the electric field by the dotted curve, plotted as a function of path length along the field line. The scale is normalized so that the magnetic field at the equator is 1 nT, roughly consistent with the observations of Manners and Masters (2019). These are all even modes (odd harmonics) with an antinode in the magnetic field at the equator, again consistent with their observations. The electric field is given in mV/m for a wave with 1 nT magnetic field at the equator. Of course, these are linear eigenmodes and so the scales can be multiplied by an arbitrary amount. The dashed line in this figure gives the local cylindrical radial distance ρ corresponding to each point in the plot.

It is perhaps a coincidence that our particular model produces periods consistent with these observations. While the model is based on statistical features of the magnetic field and plasma density based on spacecraft data, it is doubtful in any particular case that the model gives an exact

description of the magnetic field and density in any particular case. Nevertheless, the fact that resonant modes in the range of periods that are commonly observed lends support to the idea that these resonant modes are associated with the quasi-periodic pulsations observed in the Jovian magnetosphere.

4. Time domain simulations

To support and verify these eigenmode calculations, we have performed time-domain simulations, again focusing on the M = 23 field line. These simulations integrate equations (13) and (14) directly. We perform runs in which there is an initial perturbation in the equatorial electric field, which can be thought of as an imposed perturbation in the azimuthal **E×B** flow. The ionospheres in both hemispheres are set to a Pedersen conductance of 1 S. We consider two runs: one in which the initial electric field is a simple pulse, indicating a localized flow channel, and another in which there is a bipolar pulse in the electric field, corresponding to a flow shear. The first case imposes symmetry in the electric field and antisymmetry in the magnetic field, leading to the excitation of

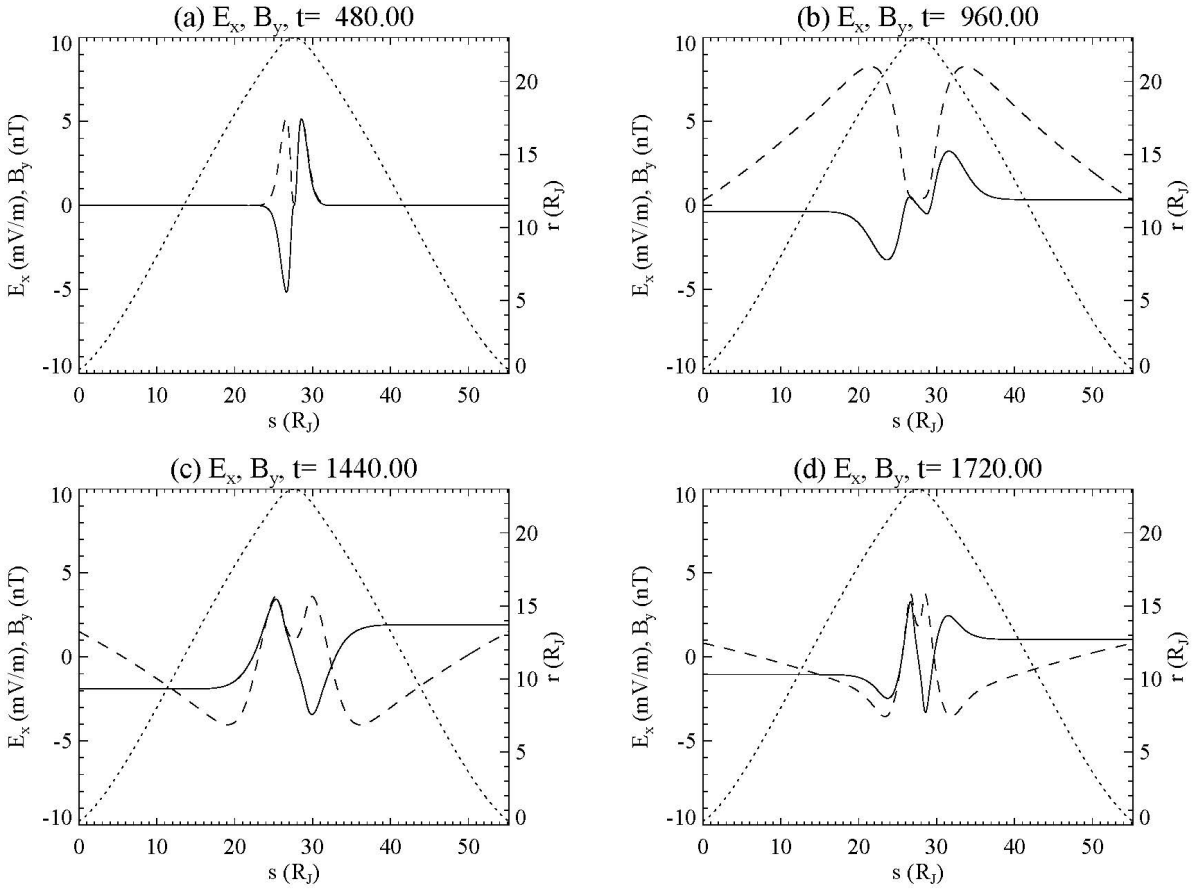

Figure 4. Snapshots of a run initialized by an electric field pulse of 10 mV/m (mapped to the ionosphere), exciting modes that are symmetric in the electric field and anti-symmetric in the magnetic field. Panels show fields at (a) 8, (b) 16, (c) 24, (d) and 32 minutes. Note all fields are mapped to the ionosphere. A full movie of this run is in the Supporting Material as Movie 1.

odd modes, while in the second case the symmetry of the electric and magnetic fields is reversed and even modes are excited. The advantage of doing an initial value problem is that the system will then be free to oscillate at its natural resonance frequencies.

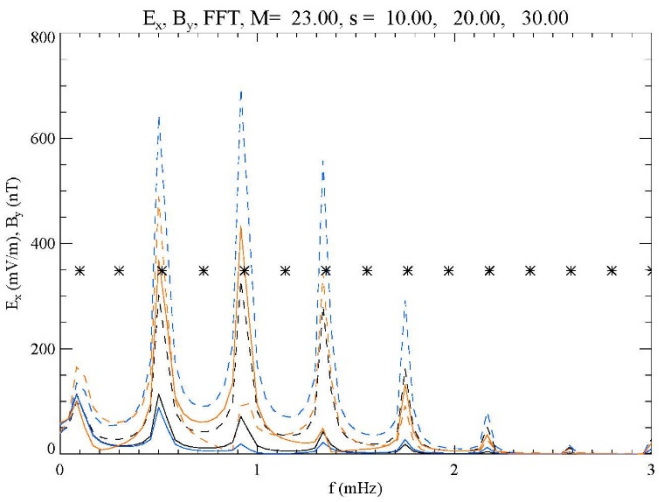

Figure 5. Spectra of the magnetic (solid curves) and electric (dashed curves) fields. These spectra are taken at distances of 10 R_J (black), 20 R_J (blue), and 30 R_J (red). Asterisks give the eigenfrequencies for this field line, showing that odd modes are excited.

Figure 4 shows snapshots every 8 minutes into a run that was initialized with a localized flow channel modeled as a Gaussian with a scale of approximately 0.4 R_J. As will be seen below, the most strongly excited mode has a period of 32 minutes, so the interval between these snapshots is one quarter of the period of this mode. The full run is shown as Movie S1 in the Supporting Material. The amplitude is 10 mV/m, mapped to the ionosphere. Both the electric and magnetic fields are mapped to the ionosphere in both this figure and the movie. Figure 5 shows the Fourier transform of the fields for this run. In this figure, the solid curves give the magnetic field spectrum and the dashed curves are the spectrum of the electric fields. The black, blue and red curves are at path lengths of 10, 20, and 30 R_J from the northern ionosphere. Figure 1 shows that 10 R_J corresponds to the high Alfvén speed region above the ionosphere, 20 R_J is at the edge of the dense plasma sheet and 30 R_J is at the equator. The asterisks in the figure correspond to the eigenfrequencies as given in Figure 2. As Figure 5 shows, the symmetry in the initial conditions allows only for the excitation of odd modes.

It should be recognized that this run was done over an artificially long time of 400 minutes, over half the Jovian rotation period, in order to get good spectral resolution; however, it is very unlikely that conditions would be stable over that period of time. With that consideration, the fundamental mode, at 167 minutes, is also unlikely to be strongly excited. On the other hand, the 3rd and 5th modes, with periods of 32 and 18 minutes, are in the range of quasi-periodic emission. It can also be seen that in the high-speed regions, the electric fields are much stronger than the magnetic fields, while the opposite is true near the equator. As a reference point, it should be noted that for a purely propagating Alfvén wave with a magnetic field amplitude of 1 nT would have an electric field of 1 mV/m if the Alfvén speed is 1000 km/s. Of course these are standing waves in which the ratio of E_α/B_β is not always equal to the Alfvén speed, as can be seen in Figure 4.

Figure 6 shows a similar run in which a shear flow channel is modeled by a bipolar pulse in the electric field. Snapshots are given at each 8 minutes for comparison with Figure 4, with the full movie included as Movie S2 in the Supporting Material. Now it can be seen that this initial condition gives a symmetric magnetic field and an antisymmetric electric field. Plots of the spectra

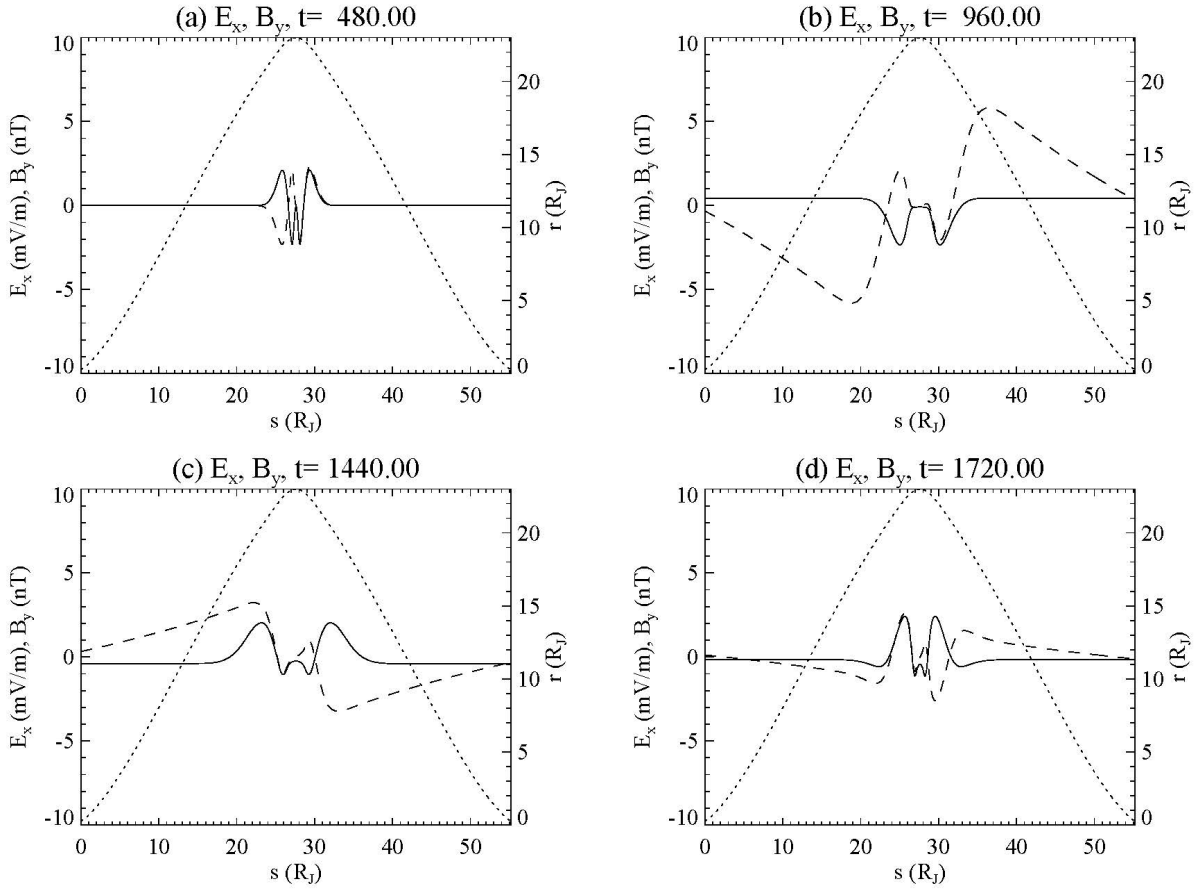

Figure 6. Snapshots from a run in which a bipolar electric field is imposed at the equator, exciting a symmetric magnetic field and an antisymmetric electric field. The panels show the fields at times of 8, 16, 24, and 32 minutes, as in Figure 4.

are given in Figure 7, using the same color and linestyle patterns as in Figure 5. Now it is clear that the even harmonics are excited by this type of impulse. It is interesting to note that the 4th and the 6th modes correspond to the 22 and 14 minute waves observed by Manners and Masters (2019).

These runs give only a few examples of the dynamics of this system. The number of harmonics excited is a function of the width of the input flow channel in the plasma sheet. For example, a run (not shown) in which the channel was one-third the size of the input for the run of Figures 4 and 5 produced stronger fields at the higher harmonics, while a broader channel only excited the low harmonics. Other runs have included driving from the ionosphere, which is potentially an important source for Alfvén wave power in the Jovian magnetosphere. Further work, including multi-dimensional simulations, will be required to fully explore the dynamics of these resonances on Jovian field lines.

5. Discussion and Conclusions

The results presented here support and extend the suggestions of Nichols et al. (2017), Manners et al. (2018) and Manners and Masters (2019) that resonant Alfvén waves can result in the quasi-periodic oscillations in the 10-40 minute range. Our model, based on the magnetic field model of

Connerney et al. (1981) and the plasma model of Bagenal and Delamere (2011), shows a rich spectrum of wave modes in this range. Time-domain simulations of a magnetic field line in Jupiter's magnetosphere show that a single pulse in the electric field, corresponding to a flow channel in the plasma sheet, can produce odd modes with electric fields symmetric about the equator and magnetic fields that are antisymmetric. Similarly, a bipolar electric field pulse, corresponding to a shear flow in the plasma sheet, produces even modes with the symmetries reversed.

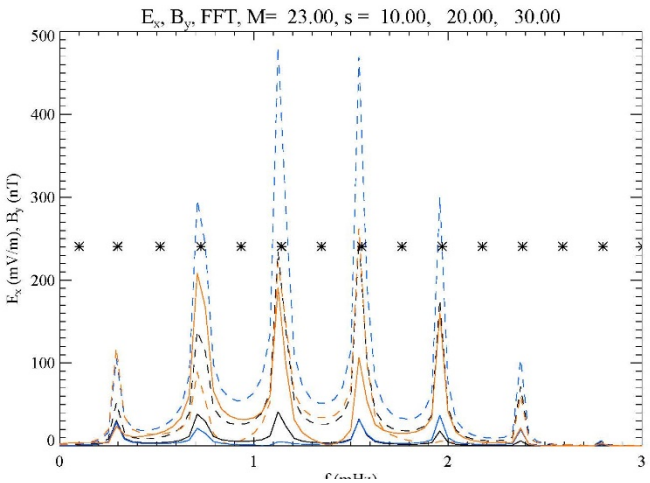

Figure 7. Spectra of the magnetic (solid) and electric (dashed) fields for the run shown in Figure 6 at distances of 10 R_J (black), 20 R_J (blue), and 30 R_J (red). In this case the even modes are excited.

However, the richness of the resonances in this range of frequencies raises the question of why particular periods seem to be favored in any given observation. The results of the time-domain simulations indicate that the spatial scales of flow channels in the plasma sheet may be responsible for picking out specific frequencies. Saur et al. (2003) have considered the formation of weak turbulence in the plasma sheet as a potential generator of field-aligned currents and Alfvén waves. Their estimate of scale lengths of 1.7 R_J is about 4 times larger than what was assumed in our simulations, which would suggest that only long-period lower harmonics would be excited. On the other hand, if wave energy cascaded to smaller scale lengths as is often the case, the shorter-period waves may come into play. Such cascades may proceed down to the ion gyroradius scale, which is estimated by Saur et al. (2018) as being about 1000 km at distances of 20-30 R_J. Such scales could produce a broad spectrum of harmonics.

Another question is how these FLR frequencies relate to the periodicities in auroral emission that are observed. The calculations presented here assume ideal MHD, in which the parallel electric field is always zero. However, kinetic effects lead to the development of parallel electric fields when the perpendicular wavelength becomes comparable to the electron inertial length or ion acoustic gyroradius (e.g., Lysak & Lotko, 1996) or when strong magnetic shears require field-aligned currents stronger than can be carried by the particles (Song & Lysak, 2006). Such scales may develop through turbulent cascade, as assumed by Saur et al. (2003, 2018); however, they may result from the propagation of the waves along the field lines. As can be seen in Figure 2, adjacent field lines have different resonant frequencies, which leads to phase mixing causing the perpendicular wavelength to decrease (e.g,. Lysak & Song, 2008; Mann et al., 1995). This can produce the time-dependent parallel electric fields that are necessary to explain the Juno observations of broadband acceleration of electrons at low altitudes above the auroral zone (e.g., Clark et al., 2018; Mauk et al., 2017).

While the present work confirms the existence of multiple field line harmonics with periods of tens of seconds, the mechanism for excitation of these waves is still an open question. As noted above, turbulence in the plasma sheet may play a major role in the development of these currents. On the other hand, in contrast to the Earth, the Jovian upper atmosphere itself can have structured flows (e.g., Yates et al., 2014) that can couple to the ionosphere through collisions and drive currents. In a dynamic situation, such flows may drive Alfvén waves that could propagate out into the magnetosphere. Given that the co-rotation of Jupiter is the major energy source for driving magnetospheric dynamics, it is reasonable to assume that the ionosphere can contribute to the input of Alfvén wave energy that can excite the field line resonances. Exploring these possibilities will be the focus of future work.

Finally, while the focus of this paper has been on the main auroral oval of Jupiter, it is well known that Alfvén wave propagation is important on the Io flux tube. Recent modeling efforts (e.g., Damiano et al., 2019; Hinton et al., 2019) have shed light on the propagation paths and kinetic effects on Alfvén waves produced by Io. It is most likely that the multiple auroral bright spots in the tail of the Io auroral emission (e.g., Szalay et al., 2018) may be associated with field line resonances of the sort we describe here. Further investigations in this area would also be useful.

In summary, we have modeled the propagation of resonant Alfvén waves on magnetic field lines associated with the main auroral oval at Jupiter. Our results show that multiple harmonics in the 10-40 minute range can be excited and may be associated with quasi-periodic auroral emissions. New observations from Juno will help us refine our model. Understanding of the dynamics of Alfvén wave propagation in the Jovian magnetosphere will enable new understanding of the physical processes in this corotation-driven magnetosphere.

Acknowledgments and Data Availability.

Work at the University of Minnesota is supported by grant AGS-1840891 from the National Science Foundation. We also acknowledge supercomputer support from the Minnesota Supercomputer Institute. Source code for the numerical simulations and data files associated with the results presented in this paper will be available at the Data Repository for the University of Minnesota (DRUM) at https://conservancy.umn.edu/drum.

References

Allegrini, F., Bagenal, F., Bolton, S., Connerney, J., Clark, G., Ebert, R. W., et al. (2017), Electron beams and loss cones in the auroral regions of Jupiter, *Geophys. Res. Lett., 44,* 7131–7139, doi:10.1002/2017GL073180.

Bagenal, F. (1983). Alfven wave propagation in the Io plasma torus. *Journal of Geophysical Research, 88*(A4), 3013–3025. https://doi.org/10.1029/JA088iA04p03013

Bagenal, F. (1994), Empirical model of the Io plasma torus: Voyager measurements, *J. Geophys. Res., 99,* 11,043–11,062, doi:10.1029/93JA02908.

Bagenal F., & P. A. Delamere (2011), Flow of mass and energy in the magnetospheres of Jupiter and Saturn, *J. Geophys. Res., 116,* A05209, doi:10.1029/2010JA016294.

Bagenal, F., Adriani, A., Allegrini, F., Bolton, S. J., Bonfond, B., Bunce, E., et al. (2014), Magnetospheric Science Objectives of the *Juno* mission, *Space Sci. Rev.,* doi: 10.1007/s11214-014-0036-8.

Belcher, J. W., Goertz, C. K., Sullivan, J. D., & Acuna, M. H. (1981). Plasma observations of the Alfvén wave generated by Io. *Journal of Geophysical Research, 30,* 8508–8512. https://doi.org/10.1029/JA086iA10p08508

Chust, T., Roux, A., Kurth, W. S., Gurnett, D. A., Kivelson, M. G., & Khurana, K. K. (2005). Are Io's Alfven wings filamented? Galileo observations. Planetary and Space Science, 53(4), 395–412. https://doi.org/10.1016/j.pss.2004.09.021

Clark, G., Tao, C., Mauk, B. H., Nichols, J., Saur, J., Bunce, E. J., et al. (2018). Precipitating electron energy flux and characteristic energies in Jupiter's main auroral region as measured by Juno/JEDI, *Journal of Geophysical Research: Space Physics, 123,* 7554–7567, . https://doi.org/10.1029/2018JA025639

Connerney, J. E. P., Acuña, M. H., & Ness N. F. (1981), Modeling the Jovian current sheet and inner magnetosphere, *J. Geophys. Res., 86,* 8370.

Connerney, J. E. P., Kotsiaros, S., Oliversen, R. J., Espley, J. R., Joergensen, J. L., Joergensen, P. S., et al. (2018). A new model of Jupiter's magnetic field from Juno's first nine orbits. *Geophysical Research Letters, 45,* 2590–2596. https://doi.org/10.1002/2018GL077312

Crary, F. J. (1997), On the generation of an electron beam by Io, *J. Geophys. Res. Space Physics, 102,* 37.

Cummings, W. D., O'Sullivan, R. J., & Coleman, P. J. (1969), Standing Alfvén waves in the magnetosphere, *J. Geophys. Res., 74,* 778.

Damiano, P. A., Delamere, P. A., Stauffer, B., Ng, C.-S., & Johnson, J. R. (2019). Kinetic simulations of electron acceleration by dispersive scale Alfvén waves in Jupiter's magnetosphere, Geophysical Research Letters, 46, 3043–3051, doi: 10.1029/2018GL081219

Dougherty L. P., Bodisch, K. M., & F. Bagenal (2017), Survey of Voyager plasma science ions at Jupiter: 2. Heavy ions, *J. Geophys. Res. Space Physics, 122,* doi:10.1002/2017JA024053.

Dunn, W. R., Branduardi-Raymont, G., Ray, L. C., Jackman, C. M., Kraft, R. P., Elsner, R. F., et al. (2017), The independent pulsations of Jupiter's northern and southern X-ray auroras, *Nature Astronomy, 1,* 758, doi: 10.1038/s41550-017-0262-6.

Gurnett, D. A., & Goertz, C. K. (1981). Multiple Alfvén wave reflections excited by Io: Origin of the Jovian decametric arcs. Journal of Geophysical Research, 86(A2), 717–722. https://doi.org/10.1029/JA086iA02p00717

Hinton, P. C., Bagenal, F., & Bonfond, B. (2019). Alfvén wave propagation in the Io plasma torus. Geophysical Research Letters, 46, 1242–1249. https://doi.org/10.1029/2018GL081472

Khurana, K., & Kivelson, M. G. (1989), Ultralow frequency MHD waves in Jupiter's middle magnetosphere, *J. Geophys. Res., 94,* 5241.

Lee, D.-H., & Lysak, R. L. (1989), Magnetospheric ULF wave coupling in the dipole model: the impulsive excitation, *J. Geophys. Res., 94,* 17,097.

Lee, D.-H., & Lysak, R. L. (1990), Effects of azimuthal asymmetry on ULF waves in the dipole magnetosphere, *Geophys. Res. Lett., 17,* 53.

Lee, D.-H., & Lysak, R. L. (1991), Impulsive excitation of ULF waves in the three-dimensional dipole model: the initial results, *J. Geophys. Res., 96,* 3479.

Lysak, R. L., & Lotko, W. (1996), On the kinetic dispersion relation for shear Alfvén waves, *J. Geophys. Res., 101,* 5085.

Lysak, R. L., & Song, Y. (2008), Propagation of kinetic Alfvén waves in the ionospheric Alfvén resonator in the presence of density cavities, *Geophys. Res. Lett., 35,* L20101, doi:10.1029/2008GL035728.

Mallinckrodt, A. J., & Carlson, C. W. (1978), Relations between transverse electric fields and field-aligned currents, *J. Geophys. Res., 83,* 1426.

Mann, I. R., Wright, A. N., & Cally, P. S. (1995), Coupling of magnetospheric cavity modes to field line resonances: a study of resonant widths, *J. Geophys. Res., 100,* 19,441.

Manners, H., Masters, A., & Yates, J. N. (2018). Standing Alfvén waves in Jupiter's magnetosphere as a source of ~10- to 60-min quasiperiodic pulsations. *Geophysical Research Letters, 45,* 8746–8754, https://doi.org/10.1029/2018GL078891

Manners, H. A., & Masters, A. (2019). First evidence for multiple-harmonic standing Alfvén waves in Jupiter's equatorial plasma sheet. Geophysical Research Letters, 46, 9344–9351. https://doi.org/10.1029/2019GL083899

Mauk, B. H., Haggerty, D. K., Paranicas, C., Clark, G., Kollman, P., Rymer, A. M., et al. (2017), Discrete and broadband electron acceleration in Jupiter's powerful aurora, *Nature, 549,* 66, doi: 10.1038/nature23648.

Nichols, J. D., Yeoman, T. K., Bunce, E. J., Chowdhury, M. N., Cowley, S. W. H., & Robinson, T. R. (2017). Periodic emission within Jupiter's main auroral oval. Geophysical Research Letters, 44, 9192–9198, https://doi.org/10.1002/2017GL074824

Press, W. H., Teukolsky, S. A., Vetterling, W. T., & Flannery, B. P. (1992), *Numerical Recipes: The Art of Scientific Computing,* 2nd edition, Cambridge University Press.

Rankin, R., Samson, J. C., Tikhonchuk, V. T., & Voronkov, I. (1999), Auroral density fluctuations on dispersive field line resonances, *J. Geophys. Res., 104,* 4399.

Saur, J., Pouquet, A., & Matthaeus, W. H. (2003), An acceleration mechanism for the generation of the main auroral oval on Jupiter, *Geophys. Res. Lett., 30,* 1260, doi: 10.1029/2002GL015761.

Saur, J., Janser, S., Schreiner, A., Clark, G., Mauk, B. H., Kollman, P., et al. (2018), Wave-particle interaction of Alfvén waves in Jupiter's magnetosphere: Auroral and magnetospheric particle acceleration. *Journal of Geophysical Research: Space Physics,* 123, 9560–9573, https://doi.org/10.1029/2018JA025948

Song, Y., & Lysak, R. L. (2006), The displacement current and the generation of parallel electric fields, *Phys. Rev. Lett*., *96,* 145002.

Streltsov, A. V., & Lotko, W. (1997), Dispersive, nonradiative field line resonances in a dipolar magnetic field geometry, *J. Geophys. Res., 102,* 27,121.

Su, Y., Jones, S. T., Ergun, R. E., Bagenal, F., Parker, S. E., Delamere, P. A., & Lysak, R. L. (2006), Io-Jupiter interaction: Alfvén wave propagation and ionospheric Alfvén resonator, *J. Geophys. Res., 111,* A06211, doi:10.1029/2005JA011252.

Szalay, J. R., Bonfond, B., Allegrini, F., Bagenal, F., Bolton, S., Clark, G.. et al. (2018), In situ observations connected to the Io footprint tail aurora, *J. Geophys. Res.: Planets, 123,* 3061, doi: https://doi.org/10.1029/2018JE005752

Tikhonchuk, V. T., & Rankin, R. (2000), Electron kinetic effects in standing shear Alfvén waves in the dipolar magnetosphere, *Phys. Plasmas, 7,* 2630.

Watanabe, H., Kita, H., Tao, C., Kagitani, M., Sakanoi, T., & Kasaba, Y. (2018), Pulsation characteristics of Jovian infrared northern aurora observed by the Subaru IRCS with adaptive optics, *Geophysical Research Letters, 45,* https://doi.org/10.1029/2018GL079411

Wilson, R. J., & Dougherty, M. K. (2000), Evidence provided by Galileo of ultra low frequency waves within Jupiter's middle magnetosphere, *Geophys. Res. Lett., 27,* 835.

Yates, J. N., Achilleos, N., & Guio, P. (2014), Response of the Jovian thermosphere to a transient pulse in solar wind pressure, *Planet. Space Sci., 91*, 27.

Figure Captions

Figure 1. Background parameters for the eigenfrequency calculation. (a) Magnetic Field; (b) Mass density; (c) Alfvén speed. Contours in each plot are magnetic field lines.

Figure 2. Eigenfrequencies as a function of M-shell for first 12 eigenmodes. (a) Frequencies in mHz; (b) Periods in minutes. Note that the fundamental mode, which has periods greater than 80 minutes for all values of M, is not shown in this panel.

Figure 3. Eigenfunctions for selected modes at M = 23 as a function of length along the field line. Solid curves give magnetic perturbations and dashed curves are electric field perturbation. The fields are normalized so that the wave magnetic field at the equator is 1 nT. The dotted curve gives the radial distance of each point, referenced to the right-hand scale. (a) Mode 4, period of 22.9 minutes; (b) Mode 6, period of 14.6 minutes; (c) Mode 12, period of 7.0 minutes; (d) Mode 22, period of 4.1 minutes.

Figure 4. Snapshots of a run initialized by an electric field pulse of 10 mV/m (mapped to the ionosphere), exciting modes that are symmetric in the electric field and anti-symmetric in the magnetic field. Panels show fields at (a) 8, (b) 16, (c) 24, (d) and 32 minutes. Note all fields are mapped to the ionosphere. A full movie of this run is in the Supporting Material as Movie 1.

Figure 5. Spectra of the magnetic (solid curves) and electric (dashed curves) fields. These spectra are taken at distances of 10 R_J (black), 20 R_J (blue), and 30 R_J (red). Asterisks give the eigenfrequencies for this field line, showing that odd modes are excited.

Figure 6. Snapshots from a run in which a bipolar electric field is imposed at the equator, exciting a symmetric magnetic field and an antisymmetric electric field. The panels show the fields at times of 8, 16, 24, and 32 minutes, as in Figure 4.

Figure 7. Spectra of the magnetic (solid) and electric (dashed) fields for the run shown in Figure 6 at distances of 10 R_J (black), 20 R_J (blue), and 30 R_J (red). In this case the even modes are excited.

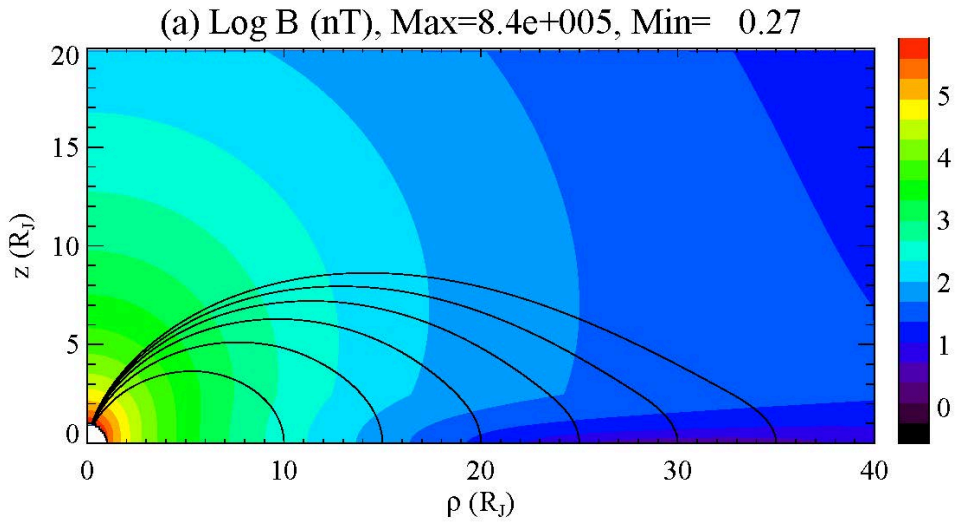
(a) Log B (nT), Max=8.4e+005, Min= 0.27
z (R_J)
ρ (R_J)
0
5
10
15
20
30
40
0
1
2
3
4
5

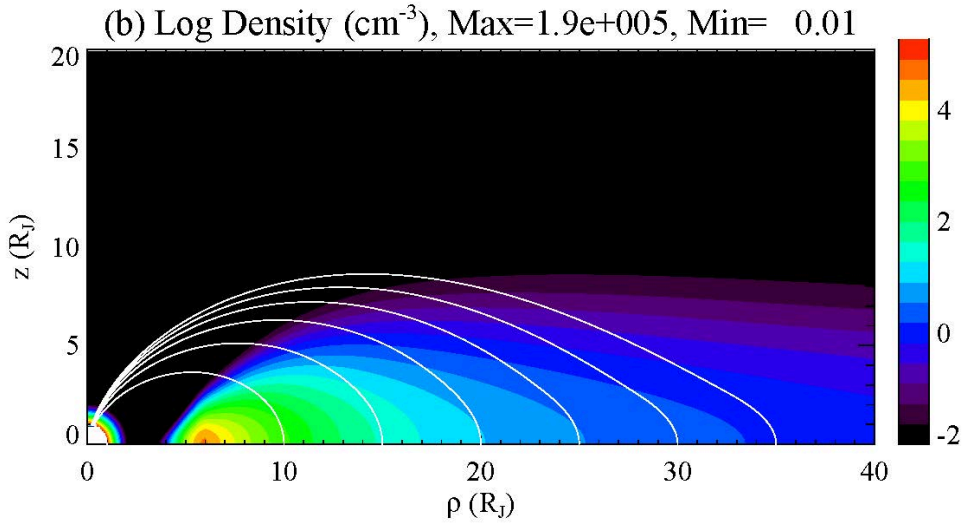
(b) Log Density (cm^-3), Max=1.9e+005, Min= 0.01
z (R_J)
ρ (R_J)
0
5
10
15
20
30
40
-2
0
2
4

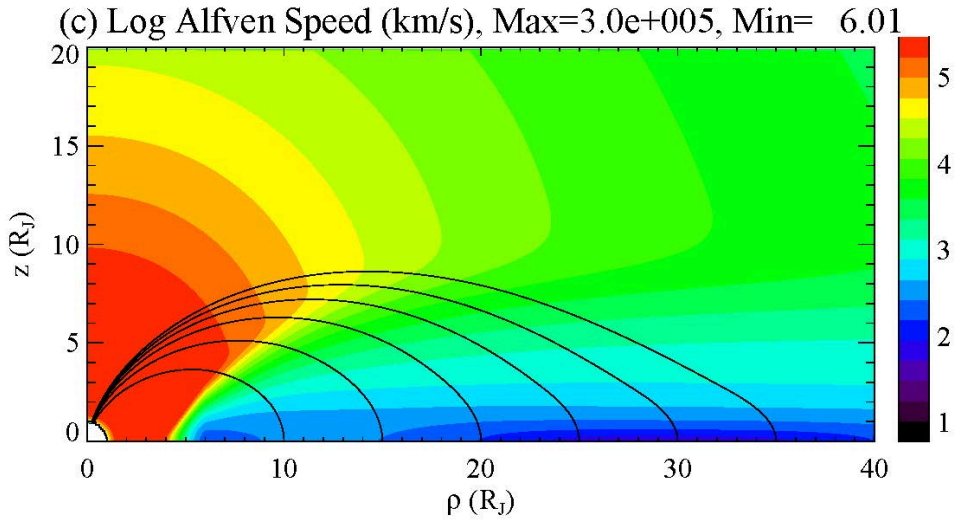
(c) Log Alfven Speed (km/s), Max=3.0e+005, Min= 6.01
z (R_J)
ρ (R_J)
0
5
10
15
20
30
40
1
2
3
4
5

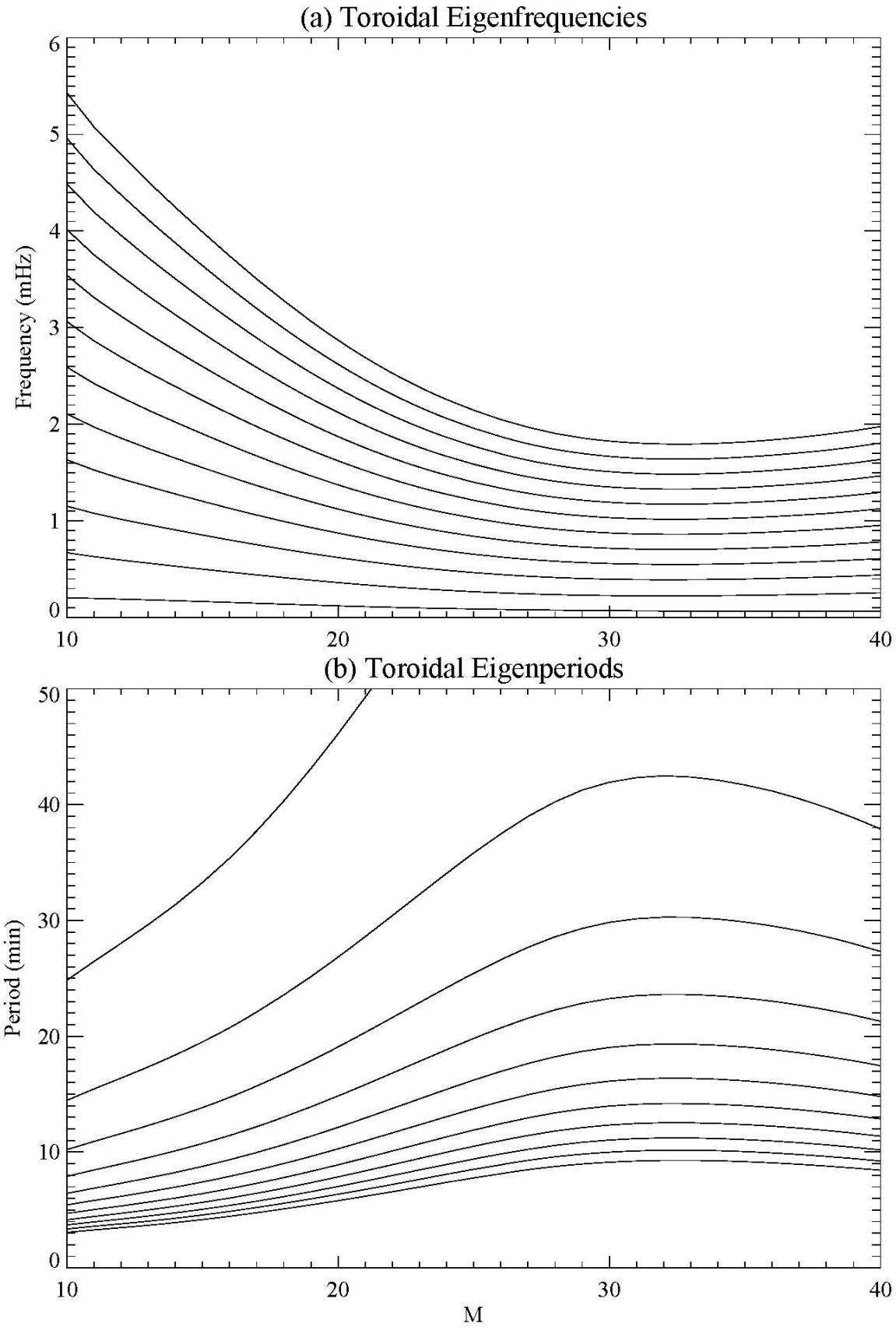
(a) Toroidal Eigenfrequencies
Frequency (mHz)
0
1
2
3
4
5
6
10
20
30
40
(b) Toroidal Eigenperiods
Period (min)
0
10
20
30
40
50
10
20
30
40
M

506 Figure 2.

507

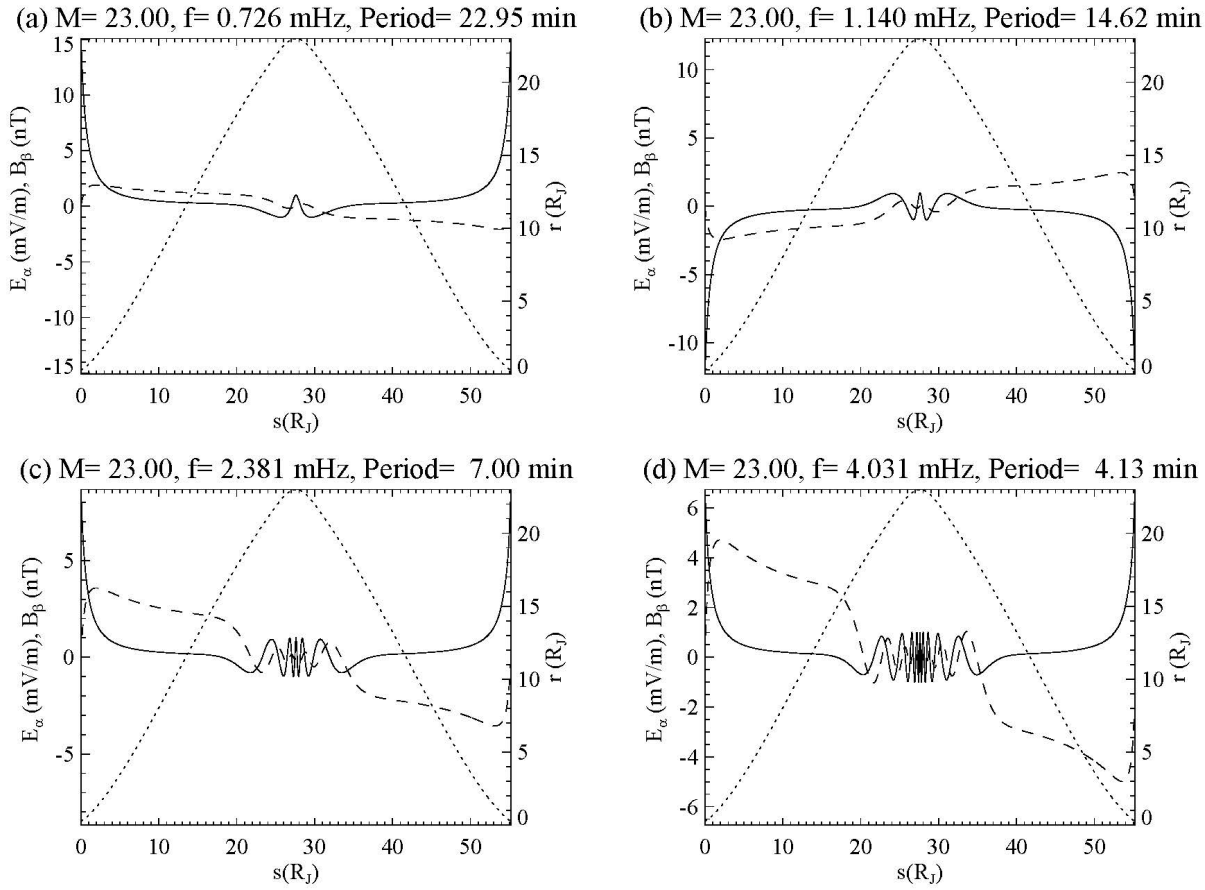

508

509 Figure 3.

510

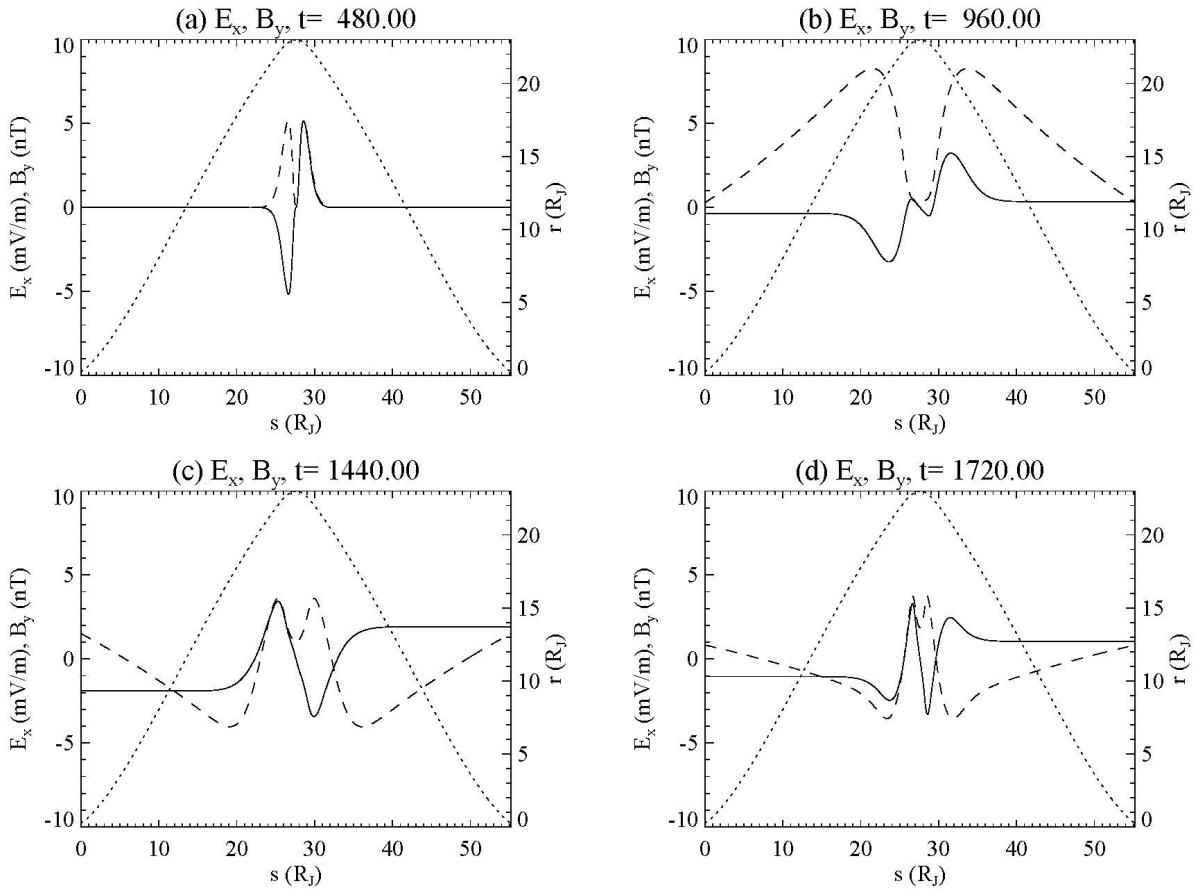

511 Figure 4.

512

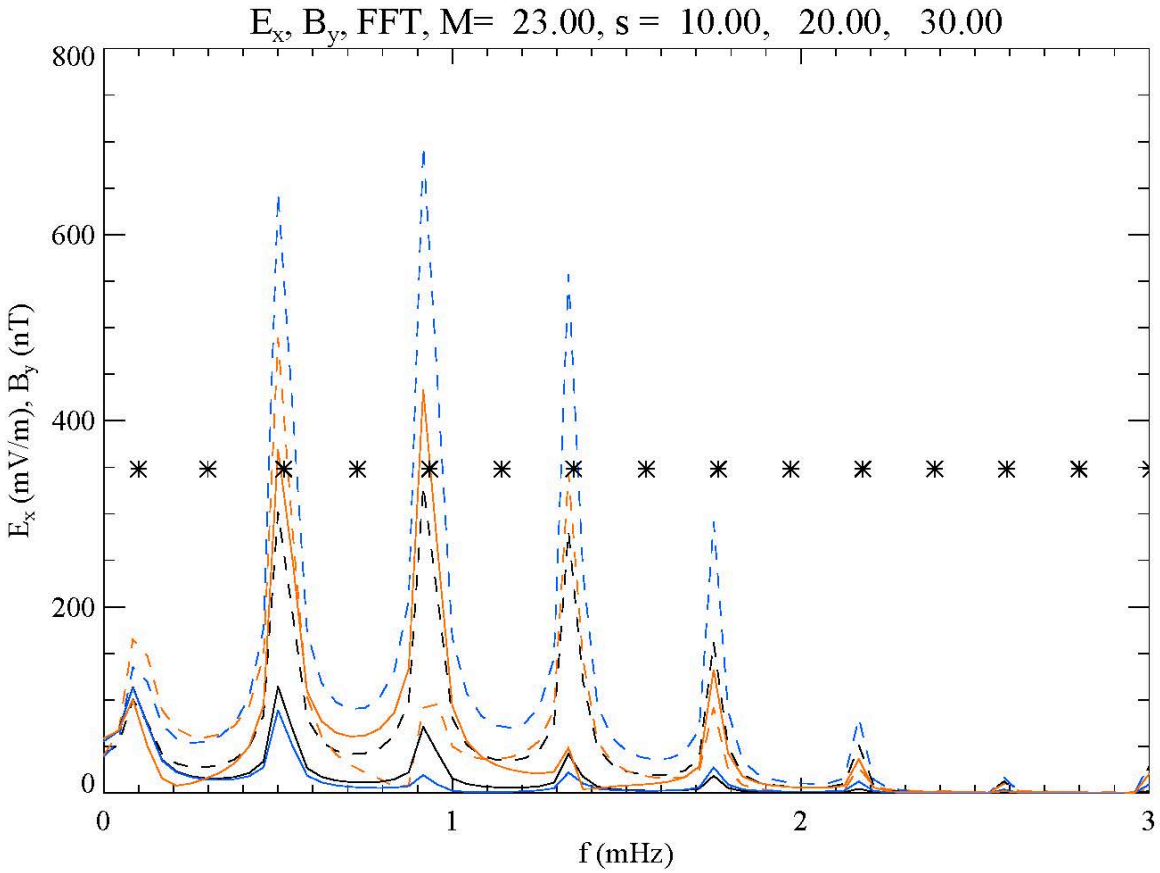

513 Figure 5.

514

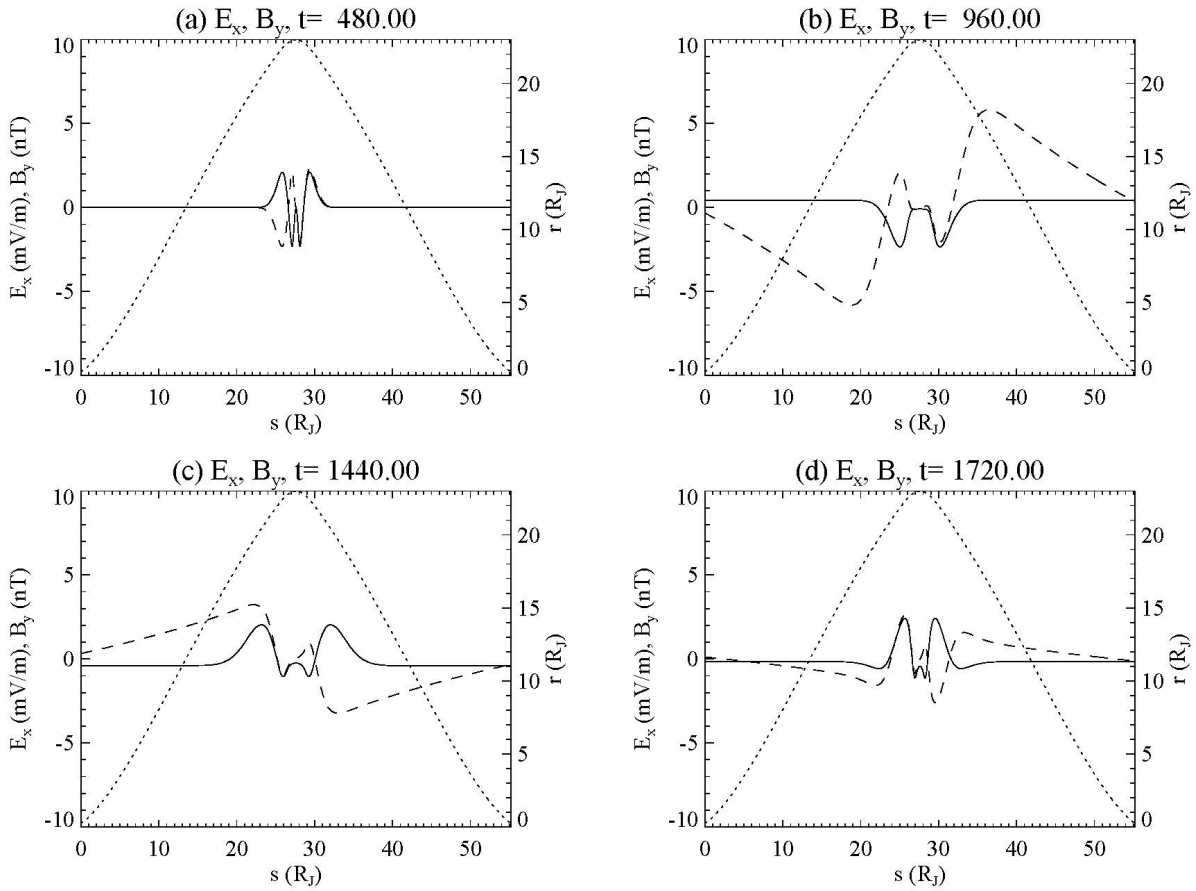

515 Figure 6.

516

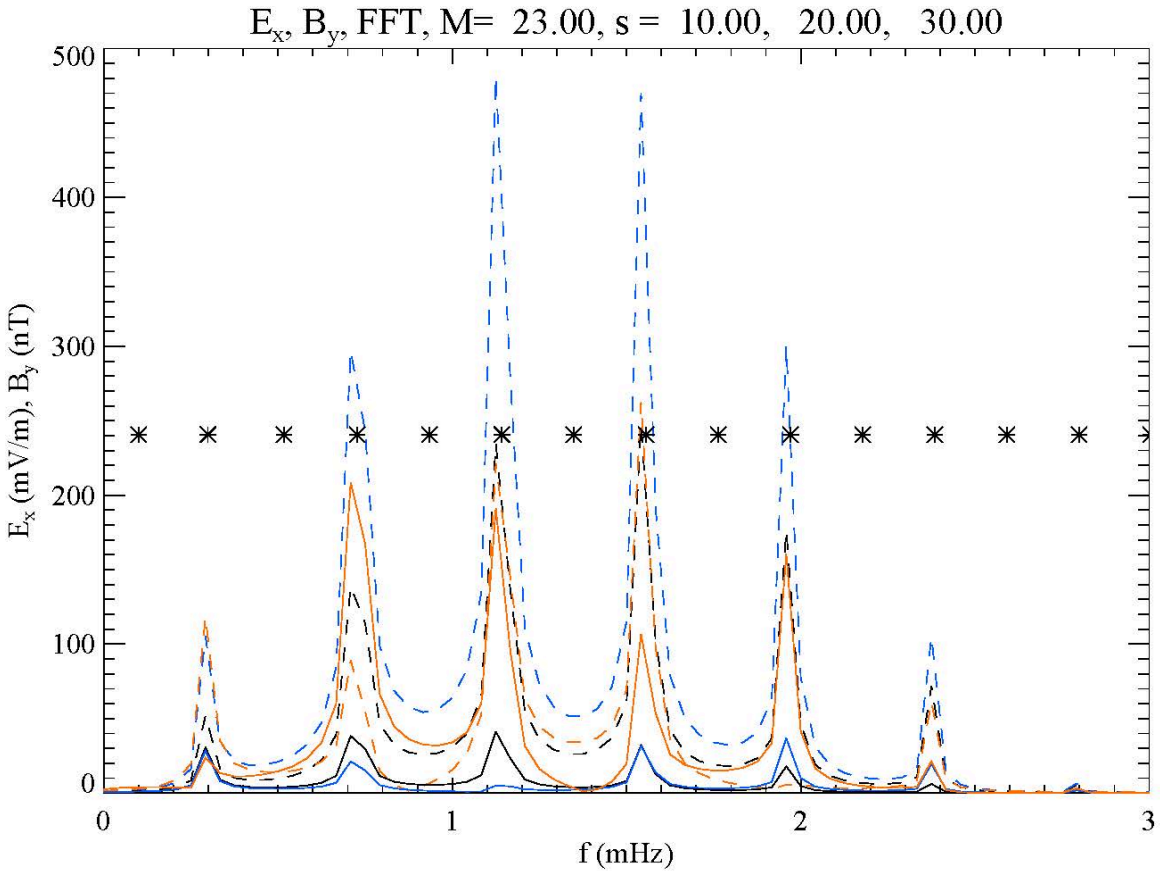

517 Figure 7.

518